AIMS Materials Science, 4(3): 551-560.
DOI: 10.3934/matersci.2017.3.551
Received: 09 March 2017
Accepted: 18 April 2017
Published: 20 April 2017

http://www.aimspress.com/journal/Materials

Research article

Solution-processed hybrid light emitting and photovoltaic devices comprising zinc oxide nanorod arrays and tungsten trioxide layers

Wei-Chi Chen, Pin-Yao Chen, and Sheng-Hsiung Yang *

Institute of Lighting and Energy Photonics, National Chiao Tung University, 301 Gaofa 3rd Road, Guiren District, Tainan City 71150, Taiwan R.O.C.

* **Correspondence:** Email: yangsh@mail.nctu.edu.tw; Tel: +886-6-303-2121; Fax: +886-6-303-2535.

Abstract: The goal of this research is to prepare inverted optoelectronic devices with improved performance by combining zinc oxide (ZnO) nanorod arrays and tungsten trioxide (WO_3) layer. ZnO seed layers with thickness of 52 nm were established, followed by growth of ZnO nanorods with length of 300 nm vertical to the ITO substrates in the precursor bath. The ZnO nanorod arrays possess high transmittance up to 92% in the visible range. Inverted light-emitting devices with the configuration of ITO/ZnO nanorods/ionic PF/MEH-PPV/PEDOT:PSS/Au were constructed. The best device achieved a max brightness and current efficiency of 10,620 cd/m^2 and 0.25 cd/A at 10 V, respectively, revealing much higher brightness compared with conventional devices using Ca/Al as cathode, or inverted devices based on ZnO thin film. By inserting a WO_3 thin layer between PEDOT:PSS and Au electrode, the max brightness and current efficiency were further improved to 21,881 cd/m^2 and 0.43 cd/A, respectively. Inverted polymer solar cells were also fabricated with the configuration of ITO/ZnO nanorods/ionic PF/P3HT:$PC_{61}BM$/PEDOT/WO_3/Au. The best device parameters, including the open-circuit voltage, short-circuit current density, fill factor, and power conversion efficiency, reached 0.54 V, 14.87 mA/cm^2, 41%, and 3.31%, respectively.

Keywords: inverted optoelectronic devices; zinc oxide; nanorod arrays; tungsten trioxide; light-emitting devices; polymer solar cells

1. Introduction

Inverted organic optoelectronic devices have drawn a lot of attention mainly due to higher

stability compared with conventional devices. The usage of air-stable metals such as gold (Au) and silver (Ag) as anode in those inverted devices consequently prolongs lifetime of devices. Furthermore, comparable or even higher device performance can be achieved by proper selection of semiconducting metal oxides, e.g., titanium dioxide (TiO_2), zinc oxide (ZnO), and molybdenum trioxide (MoO_3) serving as carrier injecting/transporting layer for construction of inverted devices. Morii et al. reported encapsulation-free hybrid organic/inorganic light-emitting diodes with the configuration of FTO/TiO_2/F8BT/MoO_3/Au [1], using TiO_2 as the electron transporting layer (ETL) and MoO_3 as the hole transporting layer (HTL). The device could be operated in air with a lower threshold voltage that provided similar luminance output compared with conventional devices using Ca/Al as cathode. Bolink et al. reported inverted light-emitting devices with the configuration of indium-tin oxide (ITO)/ZnO/Cs_2CO_3/super yellow PPV/MoO_3/Au [2], using ZnO as the ETL and Cs_2CO_3 as the hole blocking/electron injecting layer. High luminance and current efficiency of 12,000 cd/m^2 and 6.5 cd/A were achieved that is comparable with conventional devices. Park et al. proposed inverted light-emitting devices with the configuration of ITO/ZnO/Cs_2CO_3/F8BT/ poly(3,4-ethylenedioxy thiophene):poly(styrene sulfonate) (PEDOT:PSS)/Ag [3]. The Cs_2CO_3 layer was spin-cast into thin film from its solution, not by thermal evaporation. A max luminance of 3,399 cd/m^2 and max current efficiency of 0.81 cd/A around 14–16 V were obtained. Song et al. further modified device structure with the configuration of FTO/ZnO/FPQ-Br/F8BT/MoO_3/Au [4], using an ionic polyfluorene derivative FPQ-Br tethering Br^- counterions as the wetting agent to improve contact between inorganic ZnO and organic F8BT. A max luminance of 32,000 cd/m^2 and max current efficiency of 11.6 cd/A around 14 V were demonstrated. It is noted that the above metal oxide materials, including TiO_2, ZnO, and MoO_3, were applied in thin film state for those light-emitting devices; no other nanostructured type such as nanorods or nanowires has been reported yet. Recently, our group reported polymer light-emitting devices based on TiO_2 nanorods as the ETL [5]. The device was constructed with the configuration of fluorine-doped tin oxide (FTO)/TiO_2 nanorods/ionic polylfuorene (PF)/poly(2-methoxy-5-(2'-ethylhexyloxy)-1,4-phenylenevinylene) (MEH-PPV)/PEDOT:PSS/tungsten trioxide (WO_3)/Au; the max brightness and current efficiency reached 4,493 cd/m^2 and 0.66 cd/A, respectively. To the best of our knowledge, this is the first report that demonstrates inverted light-emitting devices based on TiO_2 nanorods.

Inverted device architecture has also been applied for the fabrication of organic solar cells. Hsu et al. reported inverted hybrid solar cells with the configuration of ITO/ZnO/C-PCBSD/ poly(3-hexylthiophene) (P3HT):[6,6]phenyl-C_{61}-butyric acid methyl ester ($PC_{61}BM$)/PEDOT/Ag [6], using ZnO thin film and crosslinkable fullerence derivative C-PCBSD as the ETL. The best device showed an open-circuit voltage (V_{OC}) of 0.6 V, short-circuit current density (J_{SC}) of 12.8 mA/cm^2, fill factor (*FF*) of 58%, and power conversion efficiency (*PCE*) of 4.4%, which is comparable with conventional photovoltaic devices with configuration of ITO/PEDOT/P3HT:$PC_{61}BM$/Ca/Al (V_{OC} = 0.61 V, J_{SC} = 10.6 mA/cm^2, *FF* = 67.4%, and *PCE* = 4.37%) [7]. Chen et al. reported inverted solar cells with the configuration of ITO/ZnO/PTB7-Th:$PC_{71}BM$/MoOx/Ag [8], using ZnO thin film as the ETL and an low-band-gap polymer PTB7-Th as the electron donor. The best device showed V_{OC}, J_{SC}, *FF*, and *PCE* values of 0.79 V, 14.02 mA/cm^2, 69.1%, and 7.64%, respectively. By replacing ZnO layer with a fullerene derivative-doped ZnO nanofilm, the photovoltaic property of the device was further promoted (V_{OC} = 0.8 V, J_{SC} = 15.73 mA/cm^2, *FF* = 74.3%, and *PCE* = 9.35%). In addition to ZnO film, nanostructured ZnO layer has also been applied to construct hybrid photovoltaic devices. Olson et al. reported an inverted solar device with the configuration of

ITO/ZnO nanofibers/P3HT:$PC_{61}BM$/Ag [9], using vertical grown ZnO nanofibers on ITO substrate as the ETL. However, the photovoltaic properties of the device were lowered compared with previous literatures (V_{OC} = 0.48 V, J_{SC} = 10 mA/cm^2, *FF* = 43%, and *PCE* = 2.03%). The photovoltaic performance was limited due to disordered growth and varying lengths of ZnO nanofibers verified by SEM observation. In 2014, Lin et al. reported inverted solar devices with the configuration of ITO/ZnO nanorods/PBDTTT-C-T:$PC_{71}BM$/MoO_3/Ag [10,11], using another low-band-gap polymer PBDTTT-C-T as the electron donor. More ordered ZnO nanorod arrays on the ITO substrate were demonstrated and photovoltaic properties of devices were significantly improved. The best device showed a higher *PCE* value up to 7.34%.

In this research, we demonstrate the fabrication of hybrid inverted light-emitting and photovoltaic devices comprising ZnO nanorod arrays and a WO_3 layer. WO_3 has been reported to serve as hole transporting/extraction layer for application in organic optoelectronic devices [5,12,13]. By combining electron transporting ZnO nanorod arrays and hole transporting WO_3 layers, the device performance is expected to be further improved compared with those using ZnO film as the ETL. An ionic PF material carrying hexafluorophosphate (PF_6^-) counterions as the wetting agent is also demonstrated in this study. The advantages of low temperature and solution process for deposition of ZnO, ionic PF, active materials (including MEH-PPV, P3HT, and $PC_{61}BM$), PEDOT:PSS, and WO_3 provide a promising way to low-cost optoelectronics in the future.

2. Materials and Method

2.1. Materials

The light-emitting polymer MEH-PPV was synthesized according to the literature [14]. The ionic PF carrying PF_6^- groups was synthesized according to the previous literatures and used as the wetting agent [15]. PEDOT:PSS aqueous solution (CleviosTM P VP AI 4083) was purchased from Heraeus Precious Metals GmbH & Co. KG. For photovoltaic devices, P3HT and $PC_{61}BM$ were purchased from FEM Technology Co., Inc. and used as electron donor and acceptor, respectively. The chemical structures of the above materials are shown in Figure 1. The other reagents and solvents were purchased from TCI, Aldrich, or Alfa Aesar and used without further purification.

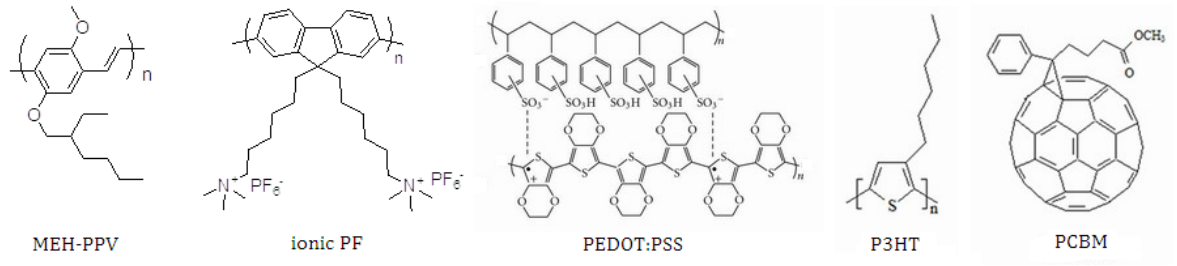

Figure 1. Chemical structures of organic materials used in this study.

2.2. Characterization

Top-view and cross-sectional scanning electron microscopy (SEM) observations were

performed with a JEOL JSM-6700F SEM instrument. The surface morphology of samples was measured by a Bruker Innova atomic force microscopy (AFM) instrument. The transmission and absorption spectra of samples were acquired at room temperature by a Princeton Instruments Acton 2150 spectrophotometer with a 150 W Xenon lamp (USHIO UXL-150S). The electrical and emission characteristics of light-emitting devices were measured in a nitrogen-purged glove box using an Agilent 4155C semiconductor analyzer and a calibrated silicon photodiode. The current density-voltage (J-V) characteristics of photovoltaic devices were taken using a Keithley 2400 source measurement unit under a simulated AM 1.5G exposure with a 1000 W Xenon Short Arc Lamp (USHIO UXL-10S). The simulated solar source was calibrated with a commercial silicon reference cell. The external quantum efficiency (EQE) measurement was conducted using a PV Measurements QEX10 instrument.

2.3. Preparation of ZnO Nanorod Arrays

The vertical growth of ZnO nanorods on arbitrary substrates covered with ZnO seed layers via the hydrothermal synthesis has been reported by Yang et al. [16]. The schematic illustration of the growth of ZnO nanorod arrays on ITO substrates is shown in Figure 2, and the detailed preparation is described as follows.

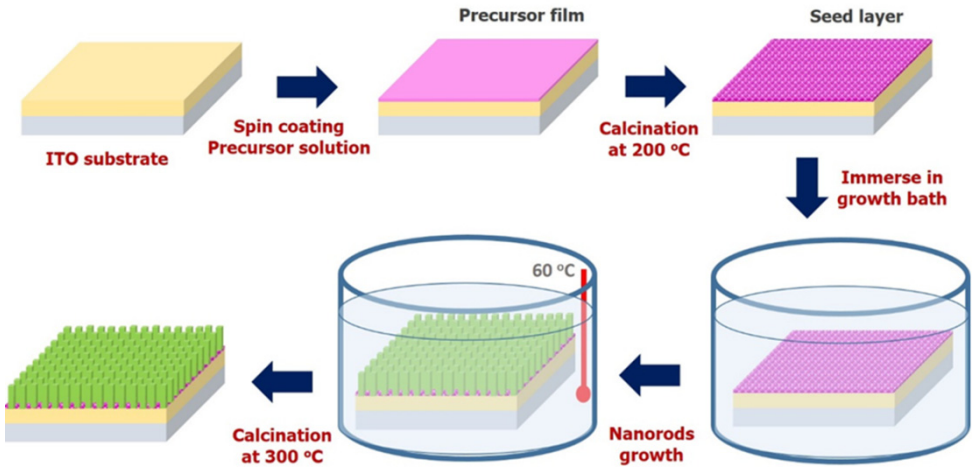

Figure 2. Schematic illustration of the growth process of ZnO nanorod arrays on the ITO substrate.

A solution of zinc acetate dihydrate (0.548 g, 2.5 mmol) in 10 mL of isopropanol (IPA) was stirred vigorously at 60 °C for 10 min. 2-(Dimethylamino)ethanol (0.223 g, 2.5 mmol) was then slowly added to the above solution and stirred at the same temperature for additional 2 hrs to form a homogeneous precursor solution. After cooling to room temperature, the precursor solution was deposited into thin film on the pre-cleaned ITO substrate by spin-coating in two steps (first step 3000 rpm/30 sec, second step 5000 rpm/20 sec), followed by calcination at 200 °C under an air atmosphere for 60 min to form a ZnO seed layer. The thickness of ZnO seed layer is about 52 nm as verified by AFM step height measurement. The next stage is to prepare ZnO nanorod arrays. A bath solution consisting of zinc sulfate heptahydrate (0.29 g, 10 mmol) and ammonium chloride (2.14 g,

400 mmol) in 150 mL of de-ionized water was prepared. 2 M sodium hydroxide (NaOH) aqueous solution was then carefully added to the above solution to adjust the pH value to 10.7, monitoring by a pH meter. The ZnO seed layers on ITO substrates were immersed in the bath solution (ZnO seed layers downward) and placed in a preheated oven (60 °C) for 45 min. The substrates were washed with de-ionized water and IPA in ultrasonic bath (10 min for each), followed by calcination at 300 °C under an air atmosphere for 30 min to form ZnO nanorod arrays. The height of ZnO nanorod arrays is about 300 nm as verified by SEM cross-sectional image. The preparation of ZnO thin film is similar to that of ZnO seed layer, followed by calcination in two steps (first step at 200 °C for 30 min, second step at 300 °C for 30 min). The thickness of ZnO thin film is about 50 nm as verified by SEM cross-sectional observation.

2.4. Device Fabrication

ITO-coated glass substrates were sequentially cleaned in detergent, de-ionized water and IPA in ultrasonic bath sequentially, followed by UV/ozone surface treatment prior to use. Inverted light-emitting devices with the configuration of ITO/ZnO nanorods/ionic PF/MEH-PPV/ PEDOT:PSS/WO_3/Au were fabricated. Ionic PF solution (1 mg in 1 mL of acetonitrile) was spin-coated on top of ZnO, followed by drying in a vacuum oven at 90 °C for 30 min. MEH-PPV film (170 nm) was spin-coated from its solution (15 mg in 1 mL of toluene) and dried in a vacuum oven at 90 °C for 30 min. PEDOT:PSS (50 nm) was spin-coated on top of MEH-PPV and baked in a vacuum oven at 90 °C for 30 min. WO_3 layer (5 nm) was prepared by spin-coating from its solution and placed in ambient environment for 15 min. Finally, Au electrodes were deposited by thermal evaporation at a base pressure of 10^{-6} torr. For photovoltaic devices, the device architecture is ITO/ZnO/ionic PF/P3HT:PC_{61}BM/PEDOT:PSS/WO_3/Au. The preparation of ZnO, ionic PF, PEDOT:PSS, WO_3, and Au electrodes were the same to the previous description. The active layer P3HT:PC_{61}BM (120 nm) was prepared by spin-coating from its solution (20 mg P3HT and 20 mg PC_{61}BM in 1 mL of *o*-DCB), followed by solvent annealing in a covered glass petridish at 60 °C for 5 min, then dried in a vacuum oven at 90 °C for 30 min.

3. Results and Discussion

3.1. Morphological Studies

The SEM micrographs of ZnO nanorod arrays from side-view and top-view are shown in Figure 3(a) and 3(b), respectively. It is seen that growth direction of ZnO nanorods is highly vertical to the ITO substrate. The length of ZnO nanorods is estimated to be 300 nm. From SEM top-view in Figure 3(b), the diameters of ZnO nanorods are in the range of 40–70 nm. It is also seen that there is still space between nanorods for materials to fill in. Due to different surface properties (ZnO is hydrophilic and organic materials are hydrophobic), an ionic PF material is proposed to serve as the wetting layer and to introduce between ZnO and organic layer. The AFM 3D-view and top-view topographic images of ZnO nanorod arrays are shown in Figure 3(c) and 3(d), respectively. The morphologies of ZnO nanorods are observed to be consistent with the SEM observation. The surface roughness (R_a) is calculated to be 16.4 nm that is far lower compared with thickness of active layers (~170 nm). The surface morphology of ZnO thin film is also investigated by SEM and AFM, as

shown in Figure 4(a) and 4(b), respectively. Homogeneous island-like crystallites are observed from SEM micrograph. Similar observation can be found from the AFM image, with a R_a value of 2.95 nm. It is concluded that ZnO thin film is well prepared and ready for device fabrication.

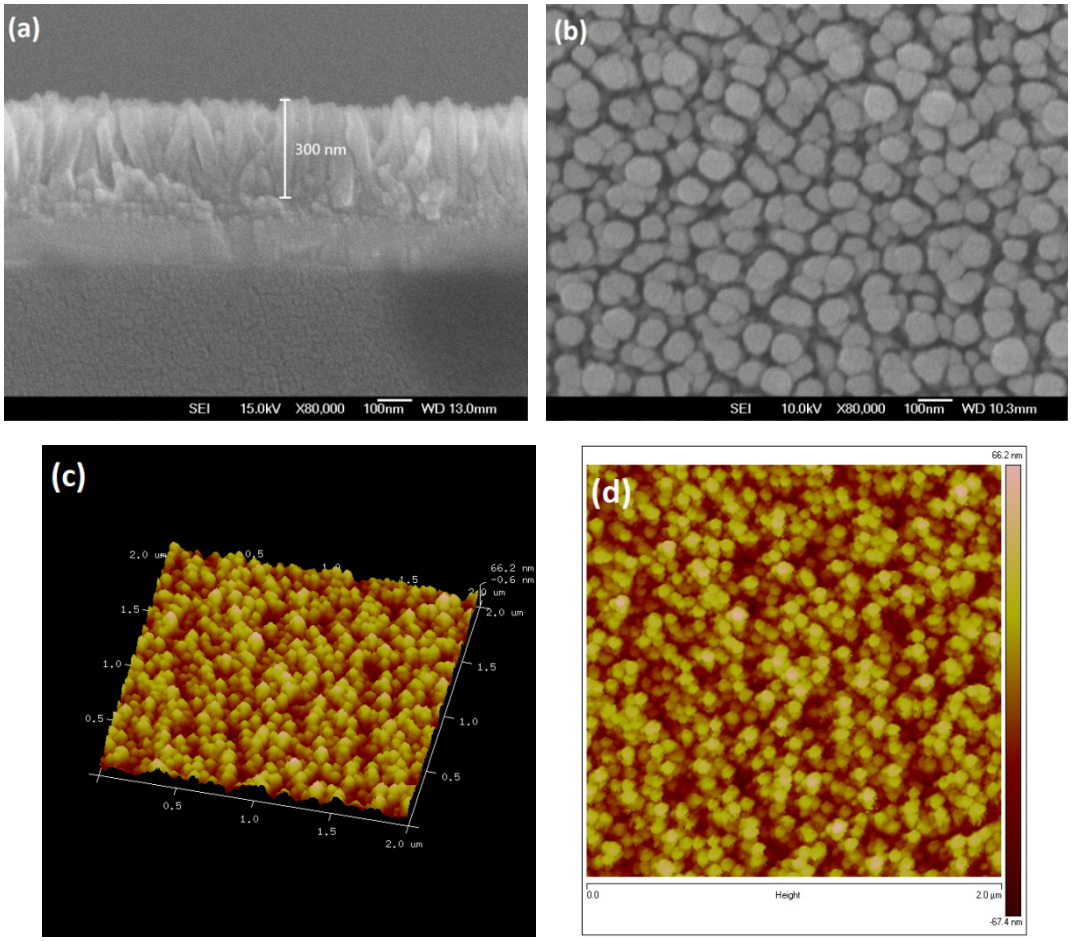

Figure 3. ZnO nanorod arrays on the ITO substrate from (a) SEM side-view, (b) SEM top-view, (c) AFM 3D-view, and (d) AFM top-view.

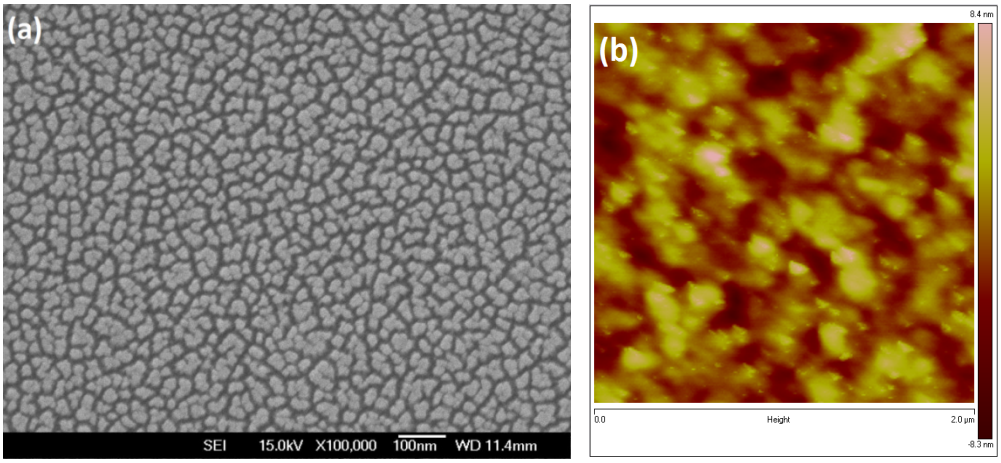

Figure 4. ZnO thin film on the ITO substrate from (a) SEM top-view and (b) AFM top-view.

3.2. Optical Properties

The UV–vis transmission and absorption spectra of ZnO thin film, nanorod arrays, and ITO substrate were measured and shown in Figure 5(a) and 5(b), respectively. It is seen that the transmittance of ZnO thin film and nanorod arrays on ITO substrate is around 92% in the visible region, which is higher than the ITO glass substrate. The observed high transmittance of ZnO layers on the ITO substrate is believed due to the antireflection effect of ZnO nanorods and film, which has been reported in the previous literatures [17,18]. The high transparent property of ZnO is especially suitable for optoelectronic applications. The main absorption band of ZnO nanorods is observed from 280 to 380 nm, which is stronger and red-shifted compared with ZnO thin film. The optical bandgaps of ZnO nanorods and film are estimated to be 3.3 eV from their absorption edge around 375 nm, which are in good accordance with previous results in the literature [19,20].

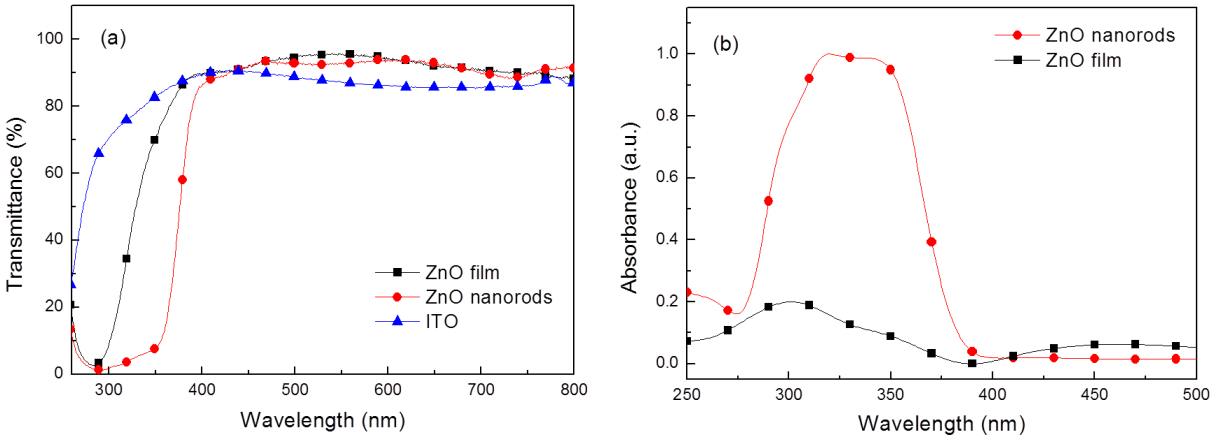

Figure 5. (a) Transmission and (b) absorption spectra of ZnO film, nanorods, and ITO substrate.

3.3. Device Performance

Inverted light-emitting devices with the configuration of ITO/ZnO/ionic PF/MEH-PPV/ PEDOT:PSS/Au were fabricated and evaluated, using ZnO as electron transporting layer, ionic PF as wetting layer, MEH-PPV as active layer, PEDOT:PSS as hole transporting layer. The performance of devices based on different types of ZnO is summarized in Table 1.

Table 1. Performance of inverted light-emitting devices based on ZnO nanorods and film.

ZnO type	Turn-on voltage (V)	Max brightness (cd/m^2)	Max current efficiency (cd/A)
thin film [a]	12.2	2,277	0.24
nanorods [a]	3.8	10,620	0.25
nanorods [b]	6.9	21,881	0.43

[a] without WO_3 layer; [b] with WO_3 layer.

The device based on ZnO nanorods showed a low turn-on voltage of 3.8 V (when luminance reached 1 cd/m^2), max brightness of 10,620 cd/m^2, and max current yield of 0.25 cd/A, revealing

much better device performance than the one based on ZnO thin film. Moreover, the brightness of the device was much higher than our previous study using TiO_2 nanorods as the ETL [5]. By inserting a thin layer of WO_3 between PEDOT:PSS and Au electrode, the max brightness and current yield were further promoted to 21,881 cd/m^2 and 0.43 cd/A, respectively. Figure 6(a) and 6(b) shows the SEM cross-sectional micrograph and snapshot of the best light-emitting device under operating bias at 10 V, respectively.

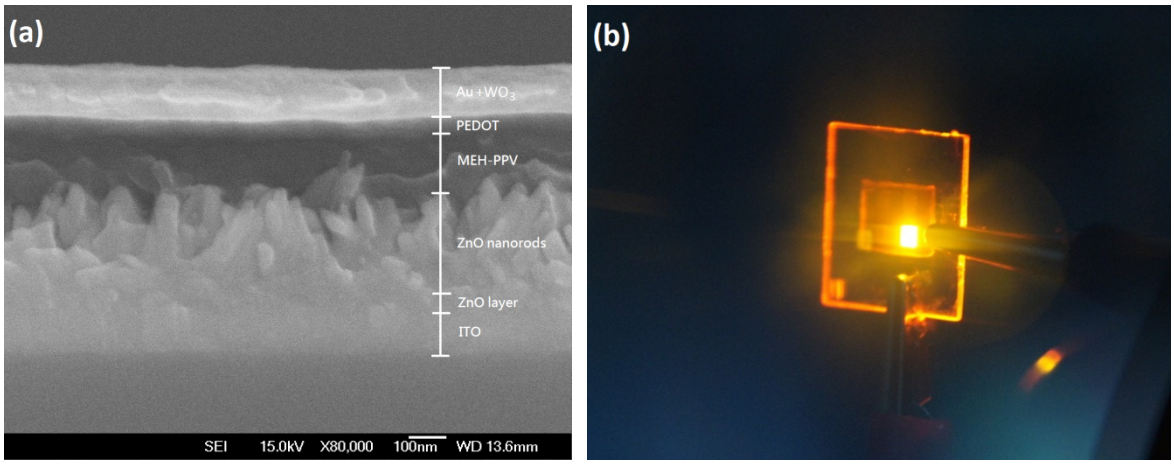

Figure 6. (a) SEM cross-sectional micrograph and (b) snapshot of the device driven at 10 V.

Inverted photovoltaic devices with the configuration of ITO/ZnO/ionic PF/P3HT:$PC_{61}BM$/PEDOT:PSS/Au were also fabricated and evaluated. As mentioned above, a thin layer of ionic PF was deposited on top of ZnO nanorods to improve contact between inorganic ZnO layer and organic P3HT:$PC_{61}BM$ layer. Moreover, a thin layer of WO_3 was inserted between PEDOT:PSS and Au electrode to act as hole extraction layer in polymer solar cells. The device parameters of photovoltaic devices based on different types of ZnO are summarized in Table 2, while the current density-voltage curves and EQE spectra of these photovoltaic devices are shown in Figure 7. It is clearly seen that the device based on ZnO nanorod arrays showed better photovoltaic properties compared with those using ZnO film as electron transporting layer. Moreover, the device comprising ZnO nanorod arrays and WO_3 layer showed the best photovoltaic properties, with V_{OC}, J_{SC}, *FF*, and *PCE* values of 0.54 V, 14.87 mA/cm^2, 41%, and 3.31%, respectively. The EQE value of the same device reached 30–40% from 400 to 650 nm, as shown in Figure 7(b). The EQE trend of the four devices is in good accordance with their photovoltaic performance, as revealed in Figure 7(a) and Table 2.

Table 2. Parameters of inverted photovoltaic devices based on ZnO nanorods and film.

ZnO type	V_{OC} (V)	J_{SC} (mA/cm^2)	*FF* (%)	*PCE* (%)
thin film [a]	0.49	10.25	34	1.74
thin film [b]	0.51	11.74	43	2.59
nanorods [a]	0.51	10.91	38	2.15
nanorods [b]	0.54	14.87	41	3.31

[a] without WO_3 layer; [b] with WO_3 layer.

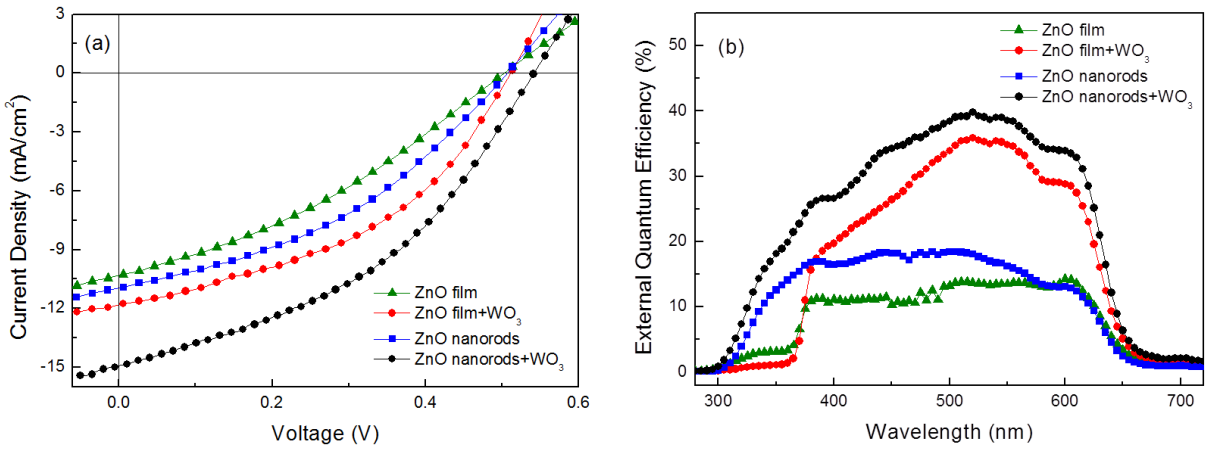

Figure 7. (a) Current density-voltage curves and (b) EQE spectra of inverted solar cells.

4. Conclusion

ZnO nanorod arrays with length of 300 nm were successfully prepared via the hydrothermal method. The growth of ZnO nanorods is highly vertical to the ITO substrate. Inverted light-emitting and photovoltaic devices based on ZnO nanorod arrays and thin film were both demonstrated. The results revealed that devices based on ZnO nanorod arrays as the ETL achieved better performance than those using ZnO thin films. Furthermore, the insertion of WO_3 layer between PEDOT:PSS and Au electrode helped to promote device performance.

Acknowledgments

The authors gratefully thank to the Ministry of Science and Technology of the Republic of China (MOST 105-2221-E-009-151) for financial support of this work.

Conflict of Interest

All authors declare no conflicts of interest in this paper.

References

1. Morii K, Ishida M, Takashima T, et al. (2006) Encapsulation-free hybrid organic-inorganic light-emitting diodes. *Appl Phys Lett* 89: 183510.
2. Bolink HJ, Coronado E, Orozco J, et al. (2009) Efficient Polymer Light-Emitting Diode Using Air-Stable Metal Oxides as Electrodes. *Adv Mater* 21: 79–82.
3. Phuong PTT, Kim NY, Jung S, et al. (2013) Improved Performance of Inverted Hybrid Light-Emitting Diodes by Post-Annealed ZnO Electron Transport Layer. *J Photonic Sci Technol* 3: 41–46.
4. Lee BR, Lee WH, Nguyen TL, et al. (2013) Highly Efficient Red-Emitting Hybrid Polymer Light-Emitting Diodes via Förster Resonance Energy Transfer Based on Homogeneous Polymer Blends with the Same Polyfluorene Backbone. *ACS Appl Mater Interfaces* 5: 5690–5695.

5. Tsai TY, Yan PR, Yang SH (2016) Solution-Processed Hybrid Light-Emitting Devices Comprising TiO_2 Nanorods and WO_3 Layers as Carrier-Transporting Layers. *Nanoscale Res Lett* 11: 516.
6. Hsieh CH, Cheng YJ, Li PJ, et al. (2010) Highly Efficient and Stable Inverted Polymer Solar Cells Integrated with a Cross-Linked Fullerene Material as an Interlayer. *J Am Chem Soc* 132: 4887–4893.
7. Li G, Shrotriya V, Huang J, et al. (2005) High-efficiency solution processable polymer photovoltaic cells by self-organization of polymer blends. *Nat Mater* 4: 864–868.
8. Liao SH, Jhuo HJ, Cheng YS, et al. (2013) Fullerene Derivative-Doped Zinc Oxide Nanofilm as the Cathode of Inverted Polymer Solar Cells with Low-Bandgap Polymer (PTB7-Th) for High Performance. *Adv Mater* 25: 4766–4771.
9. Olson DC, Piris J, Collins RT, et al. (2006) Hybrid photovoltaic devices of polymer and ZnO nanofiber composites. *Thin Solid Films* 496: 26–29.
10. Kao SH, Tseng ZL, Ho PY, et al. (2013) Significance of the ZnO nanorod array morphology for low-bandgap polymer solar cells in inverted structures. *J Mater Chem A* 1: 14641–14648.
11. Ho PY, Thiyagu S, Kao SH, et al. (2014) ZnO nanorod arrays for various low-bandgap polymers in inverted organic solar cells. *Nanoscale* 6: 466–471.
12. Tan Z, Li L, Cui C, et al. (2012) Solution-Processed Tungsten Oxide as an Effective Anode Buffer Layer for High-Performance Polymer Solar Cells. *J Phys Chem C* 116: 18626–18632.
13. Lampande R, Kim GW, Boizot J, et al. (2013) A highly efficient transition metal oxide layer for hole extraction and transport in inverted polymer bulk heterojunction solar cells. *J Mater Chem A* 1: 6895–6900.
14. Neef CJ, Ferraris JP (2000) MEH-PPV: Improved Synthetic Procedure and Molecular Weight Control. *Macromolecules* 33: 2311–2314.
15. Huang WJ, Huang PH, Yang SH (2016) PCBM doped with fluorene-based polyelectrolytes as electron transporting layers for improving the performance of planar heterojunction perovskite solar cells. *Chem Commun* 52: 13572–13575.
16. Greene LE, Law M, Tan DH, et al. (2005) General Route to Vertical ZnO Nanowire Arrays Using Textured ZnO Seeds. *Nano Lett* 5: 1231–1236.
17. Lee YJ, Ruby DS, Peters DW, et al. (2008) ZnO nanostructures as efficient antireflection layers in solar cells. *Nano Lett* 8: 1501–1505.
18. Chao YC, Chen CY, Lin CA, et al. (2010) Antireflection effect of ZnO nanorod arrays. *J Mater Chem* 20: 8134–8138.
19. So H, Senesky DG (2016) ZnO nanorod arrays and direct wire bonding on GaN surfaces for rapid fabrication of antireflective, high-temperature ultraviolet sensors. *Appl Surf Sci* 387: 280–284.
20. So H, Lim J, Suria AJ, et al. (2017) Highly antireflective AlGaN/GaN ultraviolet photodetectors using ZnO nanorod arrays on inverted pyramidal surfaces. *Appl Surf Sci* 409: 91–96.

AIMS Press